NASA Technical Memorandum 83537

Effects of Broadened Property Fuels on Radiant Heat Flux to Gas Turbine Combustor Liners

John B. Haggard, Jr.
Lewis Research Center
Cleveland, Ohio

December 1983

NASA

45 1 1 RN/NASA-TM-83537

DISPLAY 45/2/1

84N16494*# ISSUE 7 PAGE 1001 CATEGORY 34 RPT#: NASA-TM-83537

E-1906 NAS 1.15:83537 83/12/00 27 PAGES UNCLASSIFIED DOCUMENT

UTTL: Effects of broadened property fuels on radiant heat flux to gas turbine combustor liners

AUTH: A/HAGGARD, J. B., JR.

CORP: National Aeronautics and Space Administration. Lewis Research Center, Cleveland, Ohio. AVAIL.NTIS SAP: HC A03/MF A01

MAJS: /*COMBUSTION CHAMBERS/*COMBUSTION PRODUCTS/*HEAT FLUX/*JET ENGINE FUELS/* LININGS/*SOOT

MINS: / FUEL COMBUSTION/ FUEL-AIR RATIO/ GAS TURBINE ENGINES/ INLET PRESSURE/ INLET TEMPERATURE

ABA: M.G.

ABS: The effects of fuel type, inlet air pressure, inlet air temperature, and fuel/air ratio on the combustor radiation were investigated. Combustor liner radiant heat flux measurements were made in the spectral region between 0.14 and 6.5 microns at three locations in a modified commercial aviation can combustor. Two fuels, Jet A and a heavier distillate research fuel called ERBS were used. The use of ERBS fuel as opposed to Jet A under similar operating conditions resulted in increased radiation to the combustor liner and hence increased backside liner temperature. This increased radiation resulted in liner temperature increases always less than 73 C. The increased radiation is shown by way of calculations to be

ENTER:

EFFECTS OF BROADENED PROPERTY FUELS ON RADIANT HEAT FLUX TO GAS TURBINE COMBUSTOR LINERS

John B. Haggard, Jr.
National Aeronautics and Space Administration
Lewis Research Center
Cleveland, Ohio 44135

SUMMARY

The effects of fuel type, inlet air pressure, inlet air temperature, and fuel/air ratio on the combustor radiation were investigated. Combustor liner radiant heat flux measurements were made in the spectral region between 0.14 and 6.5 microns at three locations in a modified commercial aviation can combustor. Two fuels, Jet A and a heavier distillate research fuel called ERBS were used. The use of ERBS fuel as opposed to Jet A under similar operating conditions resulted in increased radiation to the combustor liner and hence increased backside liner temperature. This increased radiation resulted in liner temperature increases always less than 73° C. The increased radiation is shown by way of calculations to be the result of increased soot concentrations in the combustor. The increased liner temperatures indicated can substantially affect engine maintenance costs by reducing combustor liner life up to 1/3 because of the rapid decay in liner material properties when operated beyond their design conditions.

E-1906

INTRODUCTION

An experimental investigation was conducted to determine the effects of fuel type and combustor operating conditions on the radiant heat flux in the principle zones of a JT8-D combustor. These measurements were analyzed to determine, within the assumption of equilibrium flame temperature, the soot concentration along the length of the combustor. Knowledge of local radiant heat flux is important in the design of combustor liners. Excessive radiant heat loads to the liner require additional combustor air for liner cooling, at the expense of combustor air needed for dilution mixing, to attain a satisfactory temperature pattern factor at the turbine entrance.

With the advent of higher fuel costs as well as the potential threat of lack of availability of commercial aviation fuels, the NASA-LeRC has been engaged in a systematic research program to define and resolve potential problems in expanding the range of mid-distillate fuels which the commercial aviation industry could safely use. The use of lower quality mid distillate fuels, with increased aromatic content, causes increased liner temperatures as a result of increased radiation. Generally, the increase in liner temperature using ERBS instead of Jet A is deceptively small (usually less than 100° C). But this additional small thermal load, can substantially reduce liner life and increase maintenance costs.

The present investigation attempts to examine the effect of fuel type and combustor operating conditions on radiant heat flux. Radiant heat flux measurements were made over the wavelength interval 0.14 to 6.5 microns from which zonal averaged soot concentration measurements were calculated assuming that

local equilibrium conditions existed throughout the flow field. Tests were conducted with Jet A and an research fuel called ERBS. Combustor operating pressure varied from 27.4 to 172.9 N/cm^2, fuel-air ratios from 0.006 to 0.0161 and inlet-air temperature from 400 to 700 K. Radiant heat flux measurements were taken at three axial locations on the combustor liner wall.

ANALYSIS

A computer program was developed to model the combustion activity inside the combustor and extract estimates of local soot concentrations from the total radiometer measurements. The total radiation received by each radiometer is related to the radiation reflected or emitted by the far side of the inner combustor wall, the band radiation from the rotational and vibrational transitions of molecules of the intervening hot gas and the black body continuum radiation from discrete soot particles in the flow. The radiometer, because of the sapphire cover window, received radiation within the wavelength interval 0.14 to 6.5 μm, an interval which contains a substantial part of the total energy received. In the computer program, radiation from the liner wall was neglected since, generally, the wall is at a much cooler temperature than the gas.

It was assumed that each radiometer location in the flow was one dimensional and that chemical equilibrium existed at each radiometer site. For the purposes of calculation, 27 percent of the total air flow was assumed to be brought in upstream of primary zone radiometer site, 35 percent upstream of secondary site, and 59.5 percent upstream of the dilution site. These percentages corresponded to the actual pecentages of total open liner area available for air penetration upstream of the site reported. The local equivalence ratio at each site can be calculated by:

$$\phi_{Local} = \frac{(f/a)_{Total} / (f/a)_{Stoichiometric}}{\text{Fraction of total air brought in upstream}}$$

where $(f/a)_{Stoichiometric}$ equals 0.06824 for Jet A and 0.06924 for ERBS fuel. The local mole fractions of CO_2 and H_2O, as well as flame temperature, were calculated by knowing the local equivalance ratio using the NASA Equilibrium Program (ref. 1).

The gas band radiation modeled in the computer program involved only the local concentration of water vapor and carbon dioxide. Using the wide exponential band model of Edwards et al, references 2 - 4 (used at times beyond the temperature limit over which its been verified) a bandwidth or an equivalent wavelength interval was found for each of the major bands of CO_2 and H_2O. If A_{ij} is the bandwidth of the j^{th} band and the i^{th} gas in units of wavenumber (cm^{-1}) then

$$\bar{A}_{ij} = C_{1ij} X_i$$

$$\text{if } \beta_{ij} \leq 1 \quad \epsilon \quad A_{ij} \leq \beta_{ij} C_{3ij}$$

$$\bar{A}_{ij} = C_{2ij} (X_i Pe_{ij})^{1/2} - \beta_{ij} C_{3ij}$$

$$\text{if } \beta_{ij} \leq 1 \text{ ; } \beta_{ij} C_{3ij} < \bar{A}_{ij} \leq C_{3ij} (2 - \beta_{ij})$$

$$\bar{A}_{ij} = C_{3ij} \left[\ln \left(\frac{C_{2ij} X_i Pe_{ij}}{4 C_{3ij}^2} \right) + 2 - \beta_{ij} \right]$$

$$\text{if } \beta_{ij} \leq 1 \text{ ; } \bar{A}_{ij} > C_{3ij} (2 - \beta_{ij})$$

$$\bar{A}_{ij} = C_{1ij} X_i$$

$$\text{if } \beta_{ij} < 1 \text{ ; } \bar{A}_{ij} \leq C_{3ij}$$

$$\bar{A}_{ij} = C_{3ij} \left[\ln \left(\frac{C_{1ij} X_i}{C_{3ij}} \right) + 1 \right]$$

$$\text{if } \beta_{ij} < 1 \text{ ; } \bar{A}_{ij} \geq C_{3ij}$$

where C_{1ij}, C_{2ij}, and C_{3ij} are optical parameters that are a function of local temperature only and are reported in reference 3. The parameter β_{ij} is equal to $(C_{2ij}^2 Pe)/(4C_{1ij}C_{3ij})$. The parameter X_i is the mass path length and is equal to the product of gas density of the absorbing species for the band at test pressure and temperature times the optical path length which was held constant at 17.78 cm for the calculations.

Pe is a pressure parameter such that:

$$Pe_{ij} = \left[p_i + b_{ij} (1 - p_i) \right]^{n_{ij}}$$

where p_i is the partial pressure of the i^{th} absorbing species in atmospheres and n_{ij} and b_{ij} are optical constants specified in reference 3.

After all the bandwidths for the two absorbing species were determined at a given radiometer site and test condition and changed to wavelength intervals, del_{ij}, from wavenumbers; the bandwidths and tabulated band centers, lam_{ij}, were examined by the computer to remove any band overlaps where two bands would merge into one.

The total band radiation R_b in the wavelength interval between .14 and 6.5 μm was found by the computer technique of integration of the black body spectral emissive power over each appropriate gas band, by summing within a band in a series of 0.01 μm subintervals.

Hence,

$$R_b = \sum_i \sum_j \sum_k \frac{2\pi E_1 \ \Delta\lambda_k}{\lambda^5_{ijk} \left[\exp\left(E_2/(\lambda_{ijk} T_F)\right) - 1\right]}$$

where: k is the subinterval designator, $\Delta\lambda_k = 0.1$ μm; λ_{ijk} is the wavelength in the center of each subinterval; $E_1 = 0.5944 \times 10^{-12}$ W/cm^2 and $E_2 = 1.4388$ cm K.

The k summation was carried out over the entire bandwidth of the j band, from $lam_{ij} - del_{ij}/2$ to $lam_{ij} + del_{ij}/2$.

If R_T is the experimental total radiation heat flux measurement for a given radiometer location and given test condition and R_S is the soot component of the radiant heat flux, R_S can be expressed as the difference between the total radiation (R_T) and the band radiation (R_b).

$$R_S = R_T - R_b$$

Using the optical properties of propane soot as determined by Dalzell and Sarofim, reference 5, and a trial and error computer technique, a soot concentration was guessed and the radiation from trial soot concentration at the appropriate local test conditions was found in the wavelength interval between 0.14 and 6.5 μm, not including the gas band intervals in this region because these intervals already saturated with black body radiation have already been subtracted from the total radiation measurement. Therefore,

$$R_S = \sum_\ell \sum_k \frac{2\pi \ E_1 \ [1 - \exp(-KCS)] \ [\Delta\lambda_k]}{\lambda^5_{\ell k} \ [\exp\left(E_2/(\lambda_{\ell k} T_F)\right) - 1]}$$

where ℓ is non gas band designator in the wavelength interval 0.14 to 6.5 μm, S is the optical path length which was held constant at 17.78 cm for the calculations, C is soot volume concentration and is equal to the soot concentration divided by the density of soot (assumed to be 2 gm/cm^3) K is a spectral absorption coefficient determined by Dalzell and Sarofim (ref. 5). The following curve fit equations were used:

$$K(\lambda) = 3.8 \times 10^4 \ \lambda^{-1.48} \quad \text{if} \quad \lambda < 0.52 \ \mu m$$

$$6.23 \times 10^4 \ \lambda^{-0.7232} \quad \text{if} \quad 0.52 \ \mu m \leq \lambda \leq 1.8 \ \mu m$$

$$9.72 \times 10^4 \ \lambda^{-1.48} \quad \text{if} \quad \lambda > 1.8 \ \mu m$$

R_S trial was compared with the measured soot radiation R_S and a new estimate of soot concentration was made. This process was repeated until the resulting sum matched the measured soot radiation estimate. In this way, local soot concentration estimates were found. A summary of the computer results for the test conditions used in this study are given in table VI.

APPARATUS AND PROCEDURE

Test Facility

The test facility is shown schematically in figure 1. Laboratory-wide high pressure cold combustion air up to 25 atmospheres is supplied to this facility through flow straighteners and subsequently the flow is regulated and metered up to 10 kg/sec using an orifice. The air is then split into two legs, a cold and a hot, to gain more accurate temperature control. In the hot leg the air is passed over a natural gas fired heat exchanger. The air remains nonvitiated. The cold leg has a regulating value to apportion the split between the hot and cold leg. The two airstreams rejoin and are allowed to become well mixed before entering the test section, which houses the combustor and test instrumentation. Combustor inlet air temperatures up to 870°K are attainable with this system. A back pressure control valve downstream of a water spray controls the combustor operating pressure.

Test Section

The test section is shown in figure 2. It consisted of tubular pressure housings, the combustor, fuel lines, fuel injector, ignitor and associated instrumentation. The associated test instrumentation consisted of pressure transducers, thermocouple rakes, gas sampling probes and three hot wall radiometers, shown mounted into pressure housing in figure 3. The pressure transducers, located upstream and downstream of the combustor, sensed the combustor inlet air pressure and pressure drop through the combustor. The thermocouple rakes and gas sampling probes, whose relative locations are shown in figure 4, were located downstream of the combustor. Forty thermocouples were evenly divided onto eight rakes so that a truly representative temperature map of the exit plane could be obtained. Likewise, four gas sampling probes also spread evenly over an exit cross section were connected to gas analysis equipment which measured NO, NOx, THC, CO and CO_2.

Three total radiometers manufactured by Medtherm Corporation (Model 20) were used in the tests. As shown in figure 5, they were mounted directly (by way of a threaded boss) into the high pressure housing. The radiometers extended inside the housing along a cylinder radius so that the tips of the radiometers went into an appropriate combustor liner dilution or drilled hole and ended at the radius of the inside surface of the combustor. The radiometers are water cooled with a nitrogen purge on the outside of a sapphire window protecting the detector element. The radiometer had a 50° field of view and monitored total combustor radiation in the wavelength interval 0.14 to 6.5 μm. Each radiometer was calibrated so that the millivolt output of the device corresponded to a radiant heat flux in W/cm^2.

The combustor is a single JT8-D can of the type currently in commercial aviation service. The combustor, composed of ten rings and a dome, had louvers to provide film cooling. Each of the ten rings are labeled A through J for the purposes of the report. Ring A being the ring nearest the dome. Two thermocouples were located on the opposite exterior sides of each ring, as well as four thermocouples on the outside of the dome. These backside thermocouple locations are shown in figure 6.

Table I presents the location of the total radiometers used in this study and the spectral radiance measurement reported in reference 6. The two dilution zone radiometer locations as well as the total radiometer secondary zone location viewed combustion gases inside the combustor through standard dilution holes in the combustor liner. In the remaining three locations small nonstandard holes were drilled into the liner. Fuel was fed to the dual orifice injector in the combustor through a penetration in the high pressure housing. The fuel flows were metered using turbine flowmeters.

Fuels

Two fuels were used in this study, Jet A, the present day kerosene use by the commercial aviation fleet and research fuel called ERBS discussed in references 7 and 8. Some of the differences in fuel characteristics are shown in table II. The ERBS is a slightly poorer quality fuel as compared with Jet A in that its hydrogen content, and net heat of combustion is reduced. Only the aromatic content and sulfur content of the ERBS fuel show substantially different levels than Jet A.

RESULTS AND DISCUSSION

Collected Data

Table III to VI present the operating conditions and resulting test variables for this study of flame radiation in a modified can-annular combustor. Table III contains the combustor operating parameters and emissions data. Using the combustor inlet pressure and temperature, overall fuel-air mass ratio, and weight percent hydrogen for the Jet A and ERBS fuel; the NASA Equilibrium Computer Program (ref. 1), was used to predict the adiabatic combustor exit temperature. This was done to gain some insight and confidence into the validity of assuming chemical equilibrium throughout the combustor for the purposes of extracting soot concentration information from the total radiation measurements. These calculated adiabatic equilibrium exit temperatures were on the average 17 K$\pm$10 K above the measured average exit temperature. This result was entirely satisfactory since radial heat losses from the pressure housing were neglected in the computation. The applicability of chemical equilibrium inside the combustor closer to the fuel injector is unknown. Data was obtained over a range of inlet temperatures from 400 to 700 K, inlet pressures from 27.4 to 172 N/cm^2, and fuel-air mass ratios from 0.006 to 0.0161. Tests were run at representative combustor operating conditions.

Table IV presents the average backside liner temperatures. Each reading is the arithmatic average of the two thermocouple readings at the different circumferential positions on the indicated liner ring. The two companion run with Jet A and ERBS fuel, conducted at nearly the same fuel-air ratios are compared by substracting the benchmark Jet A test temperature from the ERBS fuel temperature. The peak temperature difference (the greatest excess ERBS temperature) of 72.6 K occurred in runs 13 and 14 at liner ring B located 12.7 cm from the injector face. The average excess ERBS temperature was 30 K$\pm$18 K.

Table V presents the fuel flow parametric measurements. A dual orifice nozzle was used in the study, to extend the operating range of the nozzle. All of the test at inlet pressures below 70 N/cm^2 were run with the primary nozzle only, while at or above 70 N/cm^2 both orifices were used. The use of two orifices may well produce a rather wide bimodal distribution of droplet sizes, with the primary nozzle producing small droplets and the secondary larger sizes. This variation together with the variation in fuel properties, ERBS fuel producing larger droplet sizes because of higher viscosity, may well be partly responsible for the elevated soot levels observed at higher pressure conditions and observed for ERBS over Jet A fuel.

Table VI presents the computer program, described in the analysis section, output results, together with the measured total radiation data in the primary, secondary, and dilution zones. It should be noted that some of the radiation data was not taken, particularly dilution zone data, and hence the analysis of that data is missing. This resulted because of a rather high rate of radiometer failure by the inadvertant melting of the solder holding the detector leads at the point where they exited the radiometer. A potential correction to the problem, as yet untried, was to enclose the leads in a stainless steel tube that stands off the radiometer base.

By simple averaging of all of the data of the ratios of ERBS total radiant heat flux measurements to the companion Jet A measurement, it was found that the ERBS fuel produced a 4 percent increase in the primary zone and an 8.4 percent increase in radiant heat flux in the secondary zone. Observing the soot concentration columns, a simple average of all of the data of the ratios of ERBS soot concentration to the companion Jet A measurement was obtained. It was found that the ERBS fuel caused a 23 percent increase in soot concentration in the primary zone and a 41 percent increase in the secondary zone.

Examination of the three columns labeled primary, secondary, and dilution zone ratio of band to soot radiation shows an experimental variation about unity with differing operating conditions. When the ratio value is less than one, soot radiation dominates over band radiation. It can be seen that soot radiation becomes most dominant over band radiation (a) in the primary zone at high inlet temperatures (620 to 700 K) and mid-range fuel-air mass ratios (0.01 to 0.0137) and (b) in the secondary zone at mid to high pressures (71 to 171 N/cm^2) and high fuel-air ratios (0.013 to 0.016).

Measured Total Radiation Behavior

The total radiation measurements in table VI are presented in figures 7, 8, and 9. They are intended to show in parametric fashion some of the radiation effects found in this experiment. In all the three figures the ERBS data fell above the Jet A data in twenty of the twenty-two unique corresponding data pairs presented.

In figure 7, flame radiation is plotted versus inlet pressure at two different inlet temperatures, 535 and 701 K and two different fuel-air mass ratios, 0.0101 and 0155. At low pressure generally the primary zone issued more radiation than the secondary zone, while the reverse is true at high pressures. The effect of pressure on flame radiation is shown to be

nonlinear. A power law formulation of the form: flame radiation α pconstant was fit to the data in figure 7. The result suggested little sensitivity of power exponent of pressure to the fuel type. The power exponents calculated 0.57 ± 0.3 are reasonable values, falling between the unity value of a optically thin volume emitter and zero for an optically thick black body emitter. The greatest difference between the ERBS and Jet A data occurred at inlet temperatures of 700 K, fuel-air mass ratios of 0.0155 and pressures of 70 to 100 N/cm^2.

Figure 8 presents radiant heat flux as a function of fuel-air mass ratio at two different pressures 33.7 and 169.4 N/cm^2 and a single inlet temperature 701 K. It can be seen that increasing the fuel-air mass ratio tends to elevate the secondary zone radiation reading more quickly than the primary zone readings. This effect may be the result of increased fuel flow causing the zone of chemical reaction to extend further downstream of the injector. The elevation of primary zone flame radiation with fuel-air mass ratio as measured is generally less than that predicted by a simple elevation in local-gas temperature as computed by the NASA Equilibrium Program as the equivalence ratio is raised at a constant total emissivity, while secondary zone flame radiation increases faster than that predicted by simple increase in equivalence ratio.

Figure 9 presents radiant heat flux as a function of inlet temperature at two different pressures 34 and 172 N/cm^2 at a constant fuel-air mass ratio of 0.0154. The increase in flame radiation with increasing inlet temperature is generally more than would be predicted by the increase in local gas temperature at constant total emissivity caused by the increase in reactant enthalpy.

It can be seen by the switch in peak radiation from the primary zone to the secondary zone as the fuel-air ratio is increased and/or the pressure is raised it appears the region of maximum burning intensity may be shifting axially downstream.

Inferred Soot Concentration Behavior

Soot concentration data were obtained by inference and not direct measurement, in a manner described in the analysis section of this report. Figure 10 presents the inferred soot concentration data plotted in semilog fashion as a function of the calculated local equilibrium temperature for three different pressure ranges, 27 to 35 N/cm^2, 71 to 105 N/cm^2, and 170 to 173 N/cm^2. The data in all three pressure ranges show in varying degrees, two trends. In the temperature region in excess of 2000 K soot concentration falls off sharply with a slope that appears to become steeper with increasing pressure. Secondly, below 2000 K in the range 1500 to 2000 K the data seem to peak at about 1 gm/m^3 in the low pressure, 4 gm/m^3 in the midpressure region and 8 gm/m^3 in the high pressure region. This behavior is similar to the studies of high temperature thermal decomposition of toluene in shock tubes (ref. 9), where the peaks in the soot yield curve occurred at about 1800 K. The current data appears rather homogenous with respect to inlet temperature and fuel type.

Figure 11 presents the behavior of inferred soot concentration plotted in a semilog fashion as a function of pressure at four different calculated average equilibrium temperatures, 1659, 1856, 2015, and 2306 K. In the lower temperature domain (fig. 11(a) and (b)), the soot concentration is greatly enhanced by increasing pressure, while only at the highest temperatures 2306 K, soot concentration is relatively insensitive to pressure.

It would seem plausible considering the last two figures presented, that one is observing a change in soot concentration behavior at or near the 2000 K temperature range caused by either or both of two phenomena. Either (a) the chemical kinetic route or rate limiting steps responsible for soot formation is abruptly curtailed as the temperature is elevated by some set of high activation energy reactions competing for the key product intermediate species necessary for soot formation, or (b) soot oxidation or burnout reactions become much more efficient in the high temperature region.

Figure 12 presents a correlation of inferred soot concentration in the secondary zone with soot concentration from SAE exhaust smoke number. The soot concentration from the SAE smoke number was calculated by using a suggested conversion in reference 10. Smoke number was converted to mass of soot per standard volume and then corrected to actual exhaust volume conditions by the perfect gas law. The result is shown in figure 12. It must be borne in mind that an exact correspondence between soot concentrations measured two different ways is not anticipated because of the different locations in the combustor where the measurements are made. There appears to be approximately a 300 fold drop in soot concentration between the front end of the secondary zone and the combustor exhaust stream. The upward slope of the data indicates the potential that the inferred soot concentration modeling effort, discussed in the analysis section, is correctly tracking changes in soot concentration. This result is similar to the results of Norgren, reference 10, who found a near 1000 fold reduction between soot in the front end of the combustor and exit conditions.

Combustor Liner Considerations

Two thermocouples were located on the backside or outside of each ring of the combustor can. Each of the two readings were arithmatically averaged. The resulting sequence of liner ring averaged temperatures described the axial temperature variation at each test condition as shown in table IV. Figure 13 presents the axial variation of the normalized backside liner temperatures for three characteristic test conditions run with Jet A fuel only. The normalization was accomplished by subtracting inlet air temperature from the averaged liner reading being plotted and dividing that result by the temperature difference between the combustor exit and inlet. From the figure it may be seen that the backside liner temperatures are, as a result of liner wall film cooling substantially below the gas exit temperatures of the combustor. The first important temperature rise is at about 13 centimeters at liner ring B. It is caused by flame radiation, conduction and convection of heat from the hot gases in the primary zone. The normalized temperature ratio for these tests varied from 0.47 to 0.17 with 0.354 ± 0.091 being the average value encountered. The data showed that at low pressure 28 N/cm^2, low fuel-air mass ratio (0.006 to 0.009), and low inlet temperature, 400 K, produced the expected lowest readings, while the highest readings occurred at the expected

maximum power conditions. Downstream of liner ring B, the normalized liner temperature ratio falls as expected, because of the lower local equivalence ratio encountered, until it reaches a minimum at liner ring E. Normalized ratios as low as 0.088 and as high as 0.279 were encountered at this station using Jet A fuel, with 0.203±0.062 being the average value. Downstream of this station the normalized temperature ratio rises to its highest level in the combustor at liner ring I, the next to last ring in the combustor. This rise may be due to poor convective cooling on the outside wall of the combustor caused by the lack of a downstream annulus air bleed and, hence, an unfavorable recirculating local flow in that part of the air annulus. This does not occur in aviation gas turbine engines. Normalized temperature ratios at ring I varied from 0.46 to 0.57 with 0.528±0.029 being the average value.

Figure 14 presents the comparisons between backside liner temperatures using Jet A and ERBS fuel. When the local liner temperature difference at each ring between Jet A and ERBS fuel was compared at nearly the same operating conditions, see table IV, it was found that nearly always the front end or primary zone of the combustor was hotter using ERBS fuel than Jet A, while the further downstream on the combustor, the more likely that the Jet A temperature data would be higher. Figure 14(a) shows at lower pressures, this axial variation with fuel-air mass ratio, a primary correlating parameter. A low fuel-air mass ratios, the domination of the ERBS fuel temperature data over the ERBS fuel temperature data over the Jet A data is limited to the front end of the combustor, while at high fuel-air ratios the ERBS temperatures are higher over nearly the entire length of the combustor. At high pressure the zone of excess radiation from ERBS fuel over Jet A covered nearly the entire liner length and was independent of fuel-air mass ratio. The magnitude of the temperature difference between the ERBS over Jet A data was, at liner ring B, where a local maximum in normalized temperature ratio exists, always less than 73 K while typically 30.3 K±18 K, see figure 14(b). At liner ring E where there is a local minimum in normalized temperature ratio, this fuel effect temperature difference is always less than 36°K while typically 13.4±10 K. Finally, at the last liner ring J, it was found that the Jet A data was nearly always higher than the ERBS data by typically 26.2±24.1 K. It was found on the average over the axial range from liner ring B to J (12.7 to 44.7 cm downstream of the injector), the ERBS temperature started 30.3 K above the Jet A liner temperature data and this run averaged temperature difference decreased 1.76 K per centimeter of downstream distance as shown in figure 14(b).

SUMMARY OF RESULTS

Radiant heat flux measurements were taken of flame emission at three locations in a modified JT8-D combustor. The following results were obtained.

(1) The ERBS fuel data as compared with Jet A data over a pressure range of 28 to 172 N/cm^2 and inlet temperatures 400 to 700 K, run at or nearly the same fuel-air mass ratio showed an average increase in total radiant heat flux to the primary zone of 4 percent and 8.4 percent in the secondary zone of the combustor.

(2) Under the assumptions of local equilibrium conditions and the assumption that the soot produced has the same optical properties as propane soot, it was found that the elevated ERBS fuel radiant heat flux was caused by an average 23 percent increase in the primary zone soot concentration and a 41 percent increase in the secondary zone soot concentration.

(3) Radiation from soot for both fuels used in this study, within the assumptions made in item no. 2, became the most dominant contributor over band radiation from H_2O and CO_2 (a) in the primary zone at high inlet temperatures (620 to 700 K) and mid range f/a ratios (0.01 to 0.0137) and (b) in the secondary zone at mid to high pressures (71 to 172 N/cm^2) and high f/a ratios (0.013 to 0.016).

(4) At lower pressures the zone of increased liner temperature resulting from the excess radiation from ERBS fuel over Jet A started in the primary zone and extended toward the dilution zone as the f/a ratio increased. At high pressure the zone of excess radiation from ERBS fuel over Jet A covered nearly the entire liner length and was independent of f/a ratio.

(5) The peak excess ERBS backside liner temperature over Jet A always occured, except at lowest f/a ratio, about 12 cm downstream of the injector face plate and was always less than 73 K higher while typically 30 ± 18 K higher. The increased temperatures indicated can reduce combustor liner life up to 1/3 primarily because of the rapid decay in liner material properties when operated beyond their design conditions.

REFERENCES

1. Gordon, S.; and McBride, B. J.: Computer Program For Calculation Of Complex Chemical Equilibrium Compositions, Rocket Performance, Incident and Reflected Shocks, and Chapman-Jouguet Detonations. NASA SP-273, Rev., 1976.

2. Siegel, Robert; and Howell, John R.: Thermal Radiation Heat Transfer, McGraw-Hill Book Co., Inc., 1972.

3. Edwards, D. K.; et al.: Radiation Heat Transfer In Nonisothermal Nongray Gases. J. of Heat Transfer, vol. 89, Aug. 1967, pp. 219-229.

4. Edwards, D. K.; and Balakrishnan, A.: Thermal Radiation By Combustion Gases. Int. J. Heat Mass Transfer, vol. 16, Jan. 1973, pp. 25-40.

5. Dalzell, W. H.; and Sarofim, A. F.: Optical Constants Of Soot And Their Application To Heat Flux Calculations. J. of Heat Transfer, vol. 91, no. 1, Feb. 1969, pp. 100-104.

6. Claus, R. W.: Spectral Flame Radiance From A Tubular-Can Combustor. NASA TP-1722, 1981.

7. Longwell, J. P., ed.: Jet Aircraft Hydrocarbon Fuels Technology. NASA CP-2033, 1978.

8. Seng, G. T.: Characterization of an Experimental Referee Broadened Specification (ERBS) Aviation Turbine Fuel and ERBS Fuel Blends. NASA TM-82883, 1982.

9. Frenklach, M.; Taki, S.; and Matula, R. A.: A Conceptual Model for Soot Formation in Pyrolysis of Aromatic Hydrocarbons. Combust. and Flame, vol. 49, nos. 1-3, Jan. 1983, pp. 275-282.

10. Norgren, C. T.: Determination of Primary-Zone Smoke Concentrations From Spectral Radiance Measurements in Gas Turbine Combustors. NASA TN D-6410, 1971.

TABLE I. - RADIOMETER AND OPTICAL ACCESS POSITIONS ON COMBUSTOR

Location		Type of penetration	Axial distance from injector face, x, cm	Cold nitrogen window purge	Angular circumvential position from top, deg
Zone	Liner ring				
Primary	A	Nonstandard-optical access (ref. 6)	5.8	Yes	300
Primary	B	Nonstandard-total radiometer	11.1	Yes	32
Secondary	D	Standard-total radiometer	16.9	Yes	0
Secondary	E	Nonstandard-optical access (ref. 6)	20.5	No	300
Dilution	G	Standard-total radiometer	27.1	Yes	0
Dilution	H	Standard-optical access (ref. 6)	32.4	No	300

TABLE II. - FUEL CHARACTERISTICS

Specifications	Jet A	ERBS
ASTM Distillation, K	411	435
Initial boiling point	451	461
10 percent evaporated	479	488
50 percent evaporated	517	552
90 percent evaporated	531	601
Specific gravity at 289 K	0.8142	0.8381
Freezing point, K	226	244
Viscosity at 250 K, (M**2/sec) *1 000 000	5	7.2
Net heat of combustion, joules/gm	43304.	42585.
Hydrogen, percent by weight	13.9	12.9
Aromatics, percent by volume	17.2	35.0
Sulfur, total percent by weight	0.020	0.085

TABLE III. - COMBUSTOR OPERATING CONDITIONS

Run number	Fuel	Inlet temperature, K	Inlet pressure, N/cm^2	Air mass flow rate, kg/sec	Fuel-air mass ratio	Combustor exit temperature K	SAE smoke number	Exit pattern factor	Emission by volume, wet, ppm				
									UHC	CO	NO	NOx	CO_2
1	JETA	401	28.0	1.84	0.0060	614		0.178	843	802	15	16	12 700
2	ERBS	401	27.4	1.80	.0060	629	20.4	.183	168	481	15	15	13 800
3	JETA	400	27.9	1.82	.0075	670		.212	841	892	14	16	15 500
4	ERBS	400	27.4	1.81	.0075	679	12.8	.212	81	354	14	17	16 100
5	JETA	401	28.0	1.85	.0089	723		.262	785	923	19	21	18 200
6	ERBS	402	27.4	1.82	.0091	745	13.5	.225	153	429	17	19	20 300
7	JETA	536	34.2	1.54	.0155	1089		.251	5	165	65	69	31 100
8	ERBS	536	34.6	1.57	.0152	1067	23.4	.216	5	124	78	81	32 600
9	JETA	699	34.2	1.17	.0102	1052	7.4	.175	2	70	77	78	21 900
10	ERBS	701	34.1	1.21	.0100	1053	10.9	.136	3	48	80	86	22 600
11	JETA	701	34.3	1.19	.0125	1133	13.5	.183	2	73	111	113	26 500
12	ERBS	702	34.1	1.19	.0124	1130		.152	2	57	135	131	27 400
13	JETA	701	34.3	1.18	.0152	1206		.185	4	74	137	143	31 400
14	ERBS	700	34.2	1.20	.0153	1220		.177	2	67	170	176	33 200
15	JETA	620	71.1	3.59	.0120	1059	28.0	.143	2	64	74	84	25 700
16	ERBS	621	71.6	3.54	.0121	1056	39.4	.234	1	60	97	109	26 900
17	JETA	621	71.2	3.58	.0137	1116		.202	5	64	88	98	29 000
18	ERBS	620	71.6	3.53	.0140	1121	43.3	.250	1	65	117	128	30 800
19	JETA	620	71.4	3.55	.0161	1197	34.6	.212	1	68	108	120	33 300
20	ERBS	620	71.7	3.56	.0159	1189	42.5	.246	1	77	128	137	35 000
21	JETA	535	102.	4.66	.0156	1092	61.3	.276	4	40	88	99	32 900
21A	JETA	537	105.	4.71	.0155	1094	55.8	.290	4	75	93	108	31 900
22	ERBS	535	104.	4.74	.0152	1088	60.0	.290	1	47	97	105	33 900
23	JETA	702	104.	3.56	.0153	1240	42.0	.231	2	34	252	267	32 600
24	ERBS	702	104.	3.53	.0155	1233	46.0	.251	2	21	246	269	33 600
25	JETA	533	170.	6.90	.0161	1108	80.6	.334	2	44	119	123	35 300
26	ERBS	534	173.	7.07	.0155	1096	77.6	.305	2	32	124	132	35 100
27	JETA	700	172.	5.88	.0101	1070	48.2	.190	2	5	169	187	23 100
28	ERBS	699	172.	5.72	.0101	1066	55.5	.193	2	32	170	195	23 200
29	JETA	700	171.	5.83	.0127	1145	47.3	.229	1	9	276	300	27 800
30	ERBS	701	172.	5.68	.0127	1149	54.5	.234	1	37	277	311	27 900
31	JETA	699.	172.	5.85	.0156	1241	54.1	.252	1	13	295	311	33 700
32	ERBS	699.	172.	5.73	.0155	1242	54.6	.261	1	45	289	326	33 200

TABLE IV. - AVERAGE BACKSIDE LINER TEMPERATURES

	Run number	Fuel	Dome temp., K @x=2.3cm	Ring A temp., K @x=5.6cm	Ring B temp., K @x=12.7cm	Ring C temp., K @x=16.3cm	Ring D temp., K @x=19.3cm	Ring E temp., K @x=22.4	Ring F temp., K @x=26.4cm	Ring G temp., K @x=30.0cm	Ring H temp., K @x=34.5	Ring I temp., K @x=40.1cm	Ring J temp., K @x=44.7cm
	1	JETA	414.4	402.1	446.1	436.2	427.2	419.7	430.6	454.0	473.8	522.3	453.0
	2	ERBS	428.3	403.4	451.8	438.1	426.9	418.7	427.2	442.1	459.3	507.2	444.3
ΔT (ERBS-JETA), K			+13.9	+1.3	+5.7	+1.9	-.3	-1.0	-3.4	-11.9	-14.5	-15.1	-8.7
	3	JETA	414.9	401.5	454.6	443.7	434.3	424.6	436.3	461.8	484.6	550.4	467.7
	4	ERBS	424.0	402.8	458.1	444.6	433.2	423.6	432.9	450.6	468.8	531.8	453.4
ΔT (ERBS-JETA), K			+9.1	+1.3	+3.5	+.9	-1.1	-1.0	-3.4	-11.2	15.8	-18.6	-14.3
	5	JETA	415.7	402.3	460.4	450.1	441.8	431.1	443.1	467.6	492.2	570.4	478.8
	6	ERBS	427.4	403.3	483.7	459.9	446.5	433.8	443.3	462.9	483.8	557.2	463.4
ΔT (ERBS-JETA), K			+11.7	+1.0	+23.3	+9.8	+4.7	+2.7	+.2	-4.7	-8.4	-13.2	-15.4
	7	JETA	598.7	545.1	705.7	680.8	671.1	646.8	656.6	671.6	695.4	807.1	685.7
	8	ERBS	614.3	548.3	742.9	717.8	705.2	674.9	670.4	671.7	698.4	782.2	633.9
ΔT (ERBS-JETA), K			+15.6	+3.2	+37.2	+37.0	+34.1	+26.1	+13.8	+.1	+3.0	-24.9	-51.8
	9	JETA	791.6	715.9	845.1	817.1	795.2	777.4	793.4	810.8	831.7	895.0	796.8
	10	ERBS	813.8	721.9	874.2	831.2	805.1	782.3	786.1	792.9	816.4	866.7	756.1
ΔT (ERBS-JETA), K			+22.2	+6.0	+29.1	+14.1	+9.9	+4.9	-7.3	-17.9	-15.3	-28.3	40.7
	11	JETA	804.0	719.3	885.1	852.5	830.5	806.2	819.0	837.6	859.8	937.6	825.3
	12	ERBS	820.6	725.6	932.2	878.8	846.2	815.9	815.9	821.1	848.4	906.3	779.2
ΔT (ERBS-JETA), K			+16.6	+6.3	+47.1	+26.3	+15.7	+9.0	-3.1	-16.5	-11.4	-31.3	-46.1
	13	JETA	809.3	722.4	921.6	888.8	869.9	841.1	851.8	865.1	884.9	973.3	836.8
	14	ERBS	825.4	727.7	994.2	943.7	909.6	869.0	861.9	879.1	863.2	952.6	805.2
ΔT (ERBS-JETA), K			+16.1	+5.3	+72.6	+54.9	+39.7	+27.9	+10.1	+14.0	-21.7	-20.7	-31.6
	15	JETA	673.0	627.3	761.3	740.6	722.3	695.3	707.9	746.2	767.6	862.5	727.5
	16	ERBS	691.9	629.3	809.1	762.8	736.9	706.3	710.4	729.2	753.7	840.1	690.7
ΔT (ERBS-JETA), K			+18.9	+2.0	+47.8	+22.2	+14.6	+11.0	+2.5	-17.0	-13.9	-22.4	-36.8
	17	JETA	675.0	629.4	783.9	760.8	747.7	719.5	730.0	762.0	787.5	895.1	753.8
	18	ERBS	691.1	628.9	830.8	791.4	773.4	738.0	739.7	754.6	779.9	870.1	702.9
ΔT (ERBS-JETA), K			+16.1	-.5	+46.9	+30.6	+25.7	+18.5	+9.7	-7.4	-7.6	-25.0	-50.8
	19	JETA	675.4	629.4	809.3	786.2	775.4	747.2	758.3	784.7	811.7	936.8	781.7
	20	ERBS	690.3	629.3	843.3	814.5	801.4	771.8	775.3	786.7	813.3	900.9	715.2
ΔT (ERBS-JETA), K			+14.9	-.1	+34.0	+28.3	+26.0	+24.6	+17.0	+2.0	+1.6	-35.9	-66.5
	21	JETA	597.4	541.2	733.3	705.2	698.2	668.4	681.6	690.3	708.7	805.3	658.6
	22	ERBS	606.8	542.0	772.5	745.6	739.7	703.9	711.1	712.2	718.7	797.6	656.8
ΔT (ERBS-JETA), K			+9.4	+.8	+39.2	+40.4	+41.5	+35.5	+29.5	+21.5	+10.0	-7.7	-1.8
	21A	JETA	598.1	544.6	736.6	716.2	708.5	674.4	681.5	688.3	707.9	806.6	613.2
	22	ERBS	606.8	542.0	772.5	745.6	739.7	703.9	711.1	712.2	718.7	797.6	656.8
ΔT (ERBS-JETA), K			+8.7	+2.6	+35.9	+29.4	+31.2	+29.5	+29.5	+23.9	+10.8	-9.0	+43.6
	23	JETA	783.4	712.8	945.5	909.5	891.3	854.2	852.1	863.6	892.7	974.6	833.4
	24	ERBS	794.8	714.9	975.5	937.7	914.4	875.8	870.6	878.2	907.3	983.1	798.1
ΔT (ERBS-JETA), K			+11.4	+2.1	+30.0	+28.2	+23.1	+21.6	+18.5	+14.6	+14.6	+8.5	-35.3
	25	JETA	601.3	539.0	745.9	721.3	714.7	681.7	699.3	709.6	711.9	799.2	609.5
	26	ERBS	607.4	539.1	758.6	735.9	728.8	690.2	706.1	715.3	715.2	792.3	627.9
ΔT (ERBS-JETA), K			+6.1	+.1	+12.7	+14.6	+14.1	+8.5	+6.8	+5.7	+3.3	-6.9	+18.4
	27	JETA	771.4	707.8	874.6	824.3	796.7	766.8	772.5	793.6	812.6	890.8	784.9
	28	ERBS	779.7	707.3	891.7	836.3	804.9	771.1	775.3	794.9	814.2	887.1	769.7
ΔT (ERBS-JETA), K			+8.3	-.5	+17.1	+12.0	+8.2	+4.3	+2.8	+1.3	+1.6	-3.7	-15.2
	29	JETA	774.6	708.6	904.6	856.3	829.7	795.4	797.8	817.3	835.4	933.6	806.7
	30	ERBS	786.8	710.4	926.7	875.2	845.5	807.1	807.3	824.2	843.1	932.3	790.6
ΔT (ERBS-JETA), K			+11.8	+1.8	+22.1	+18.9	+15.8	+11.7	+9.5	+6.9	+7.7	-1.3	-16.1
	31	JETA	775.9	707.1	914.2	885.1	869.2	836.2	840.1	854.8	871.8	976.2	831.9
	32	ERBS	786.1	707.8	932.8	902.5	884.4	848.8	852.6	864.8	881.2	972.4	802.2
ΔT (ERBS-JETA), K			+10.2	+.7	+18.6	+17.4	+15.2	+12.6	+12.5	+10.0	+9.4	-3.8	-29.7

TABLE V. - COMBUSTOR FUEL FLOW PARAMETERS

Run number	Fuel	Fuel temp., K	Total fuel mass flow rate gm/sec	Pressure drop across primary nozzle, N/cm^2	Pressure drop across secondary nozzle, N/cm^2	Fraction of fuel flowing in primary nozzle
1	JETA	305	11.1	88.1		1.00
2	ERBS	305	10.9	81.4		1.00
3	JETA	305	13.7	137.		1.00
4	ERBS	305	13.6	125.		1.00
5	JETA	304	16.6	201.		1.00
6	ERBS	303	16.6	194.		1.00
7	JETA	306	23.9	444.		1.00
8	ERBS	309	23.9	412.		1.00
9	JETA	321	11.9	114.		1.00
10	ERBS	322	12.1	111.		1.00
11	JETA	320	14.9	177.		1.00
12	ERBS	327	14.9	170.		1.00
13	JETA	313	18.2	261.		1.00
14	ERBS	330	18.4	258.		1.00
15	JETA	321	43.6	352.	6.3	.488
16	ERBS	311	42.9	309.	7.5	.478
17	JETA	314	49.2	346.	12.7	.425
18	ERBS	310	49.6	293.	16.0	.401
19	JETA	321	57.4	337.	22.9	.361
20	ERBS	309	57.0	285.	27.3	.344
21	JETA	313	73.0	272.	53.3	.265
21A	JETA	312	73.1		117.	0.00
22	ERBS	313	72.5	478.	43.8	.363
23	JETA	312	54.5	305.	28.2	.359
24	ERBS	311	54.8	262.	26.6	.339
25	JETA	308	111.	296.	183.	.184
26	ERBS	310	110.	317.	159.	.195
27	JETA	312	59.2	227.	39.9	.283
28	ERBS	312	57.8	193.	35.0	.271
29	JETA	311	73.8	207.	66.5	.223
30	ERBS	312	72.0	180.	61.5	.216
31	JETA	310	91.7	241.	110.	.195
32	ERBS	311	89.2	221.	102.	.192

TABLE VI. - COMPUTER PROGRAM RADS OUTPUT SUMMARY

Run number	Fuel	Pressure, atm	Primary zone					Secondary zone					Dilution zone				
			Equilibruim temperature, K	Measured radiation, W/cm^2	Inferred soot concentration, g/m^3	Total primary zone radiation, W/cm^2	Ratio band to soot radiation in primary zone	Equilibruim temperature, K	Measured radiation, W/cm^2	Inferred soot concentration, gm/m^3	Total secondary zone radiation, W/cm^2	Ratio band to soot radiation in secondary zone	Equilibrium temperature, K	Measured radiation, W/cm^2	Inferred soot concentration, gm/m^3	Total dilution zone radiation, W/cm^2	Ratio band to soot radiation in dilution zone
1	JETA	2.76	1222	2.58	0.679	2.83	1.27	1052	1.35	0.759	1.53	1.45	799	0.66	3.10	0.790	0.600
2	ERBS	2.70	1212	2.57	.754	3.09	1.36	1044	1.53	1.14	1.72	.993	793				
3	JETA	2.76	1398	3.53	.338	4.34	2.29	1197	2.10	.526	2.34	1.66	892	.85	1.66	.990	.905
4	ERBS	2.70	1386	3.08	.262	3.78	2.82	1186	2.28	.716	2.77	1.48	885				
5	JETA	2.76	1553	4.15	.136	5.18	4.46	1325	2.72	.308	3.44	2.79	976	1.06	1.00	1.21	1.26
6	ERBS	2.70	1561	4.42	.172	5.33	3.33	1331	3.59	.617	4.23	1.36	980				
7	JETA	3.38	2261	21.9	.236	25.6	1.34	1962	20.1	.614	21.0	.611	1451	6.42	.869	6.89	.813
8	ERBS	3.42	2225	23.2	.303	26.6	1.08	1925	23.7	.939	24.5	.440	1424				
9	JETA	3.38	1911	22.7	.942	23.5	.426	1673	12.3	.913	12.9	.564	1307	5.02	1.44	5.36	.565
10	ERBS	3.37	1879	23.8	1.16	25.8	.433	1645	10.3	.762	10.8	.671	1288				
11	JETA	3.38	2123	32.2	.770	35.0	.492	1856	19.2	.883	20.0	.476	1429	7.34	1.32	7.77	.536
12	ERBS	3.37	2100	32.8	.859	35.3	.446	1835	16.7	.756	18.5	.649	1415				
13	JETA	3.38	2332	39.2	.546	42.8	.549	2055	28.7	.809	31.3	.504	1567	10.5	1.16	11.0	.518
14	ERBS	3.37	2326	42.0	.623	45.3	.478	2048	31.1	.948	33.5	.432	1562				
15	JETA	7.03	2026	41.1	1.43	42.9	.446	1756					1336				
16	ERBS	7.06	2020	46.1	1.82	47.9	.371	1750	31.4	3.12	32.8	.337	1331				
17	JETA	7.03	2177	48.4	1.08	50.5	.483	1888					1425				
18	ERBS	7.06	2187	48.5	1.05	50.5	.484	1897	48.0	3.64	49.7	.273	1430				
19	JETA	7.03	2359	53.0	.659	55.5	.665	2064					1548				
20	ERBS	7.06	2333	47.0	.600	49.3	.681	2035	64.1	3.41	66.1	.251	1526				
21	JETA	10.19	2281	39.1	.444	41.8	1.12	1971	61.4	4.28	63.7	.284	1456				
21A	JETA	10.19	2273	38.8	.450	41.6	1.12	1964	62.7	4.78	65.0	.273	1451				
22	ERBS	10.26	2235	41.7	.615	44.4	.857	1926	70.1	12.4	72.7	.216	1424				
23	JETA	10.23	2356	55.5	.651	58.5	.805	2065	70.1	3.56	72.6	.273	1573				
24	ERBS	10.21	2357	62.2	.827	65.1	.637	2065	80.5	5.38	83.0	.225	1572				
25	JETA	16.82	2322	45.1	.370	49.2	1.78	2009	80.5	8.55	83.7	.308	1481				
26	ERBS	17.06	2262	47.6	.567	51.4	1.25	1949	86.6	27.	90.	.24	1439				
27	JETA	16.96	1902	58.9	5.97	61.6	.340	1665	30.1	4.56	32.1	.444	1301				
28	ERBS	16.96	1889	64.0	11.1	66.8	.267	1653	31.6	5.90	33.5	.382	1293				
29	JETA	16.96	2148	68.0	2.01	71.3	.492	1872	54.6	5.82	57.2	.350	1440				
30	ERBS	16.96	2133	73.2	2.58	76.5	.415	1859	58.6	9.59	61.2	.300	1430				
31	JETA	16.96	2384	61.0	.615	65.2	1.05	2087	87.6	5.77	90.9	.308	1587				
32	ERBS	16.96	2363	66.1	.810	70.2	.813	2066	94.4	12.1	97.8	.259	1572				

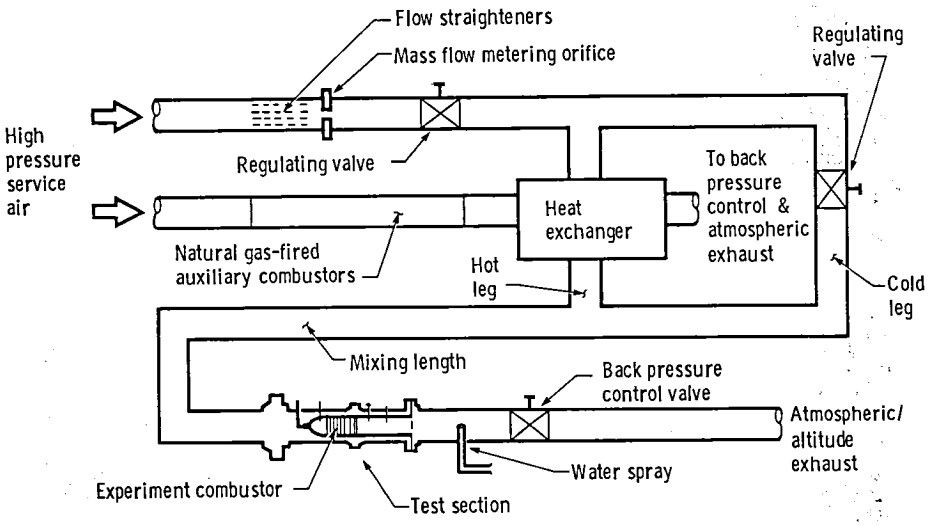

Figure 1. - Test facility and auxiliary equipment.

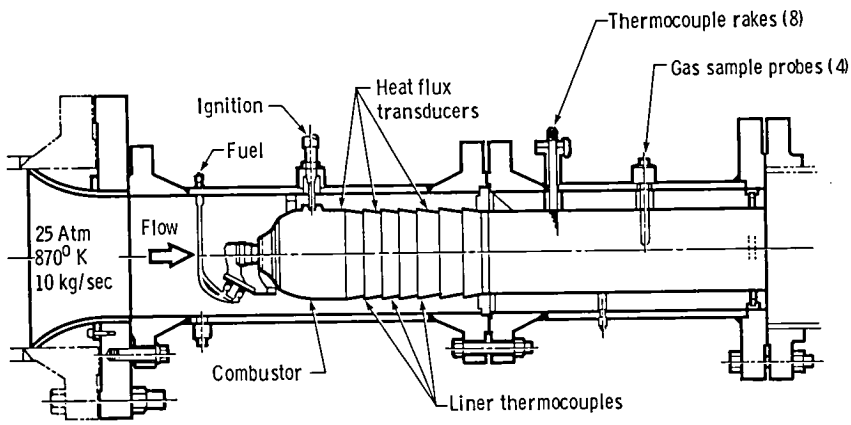

Figure 2. - Tubular combustion test section.

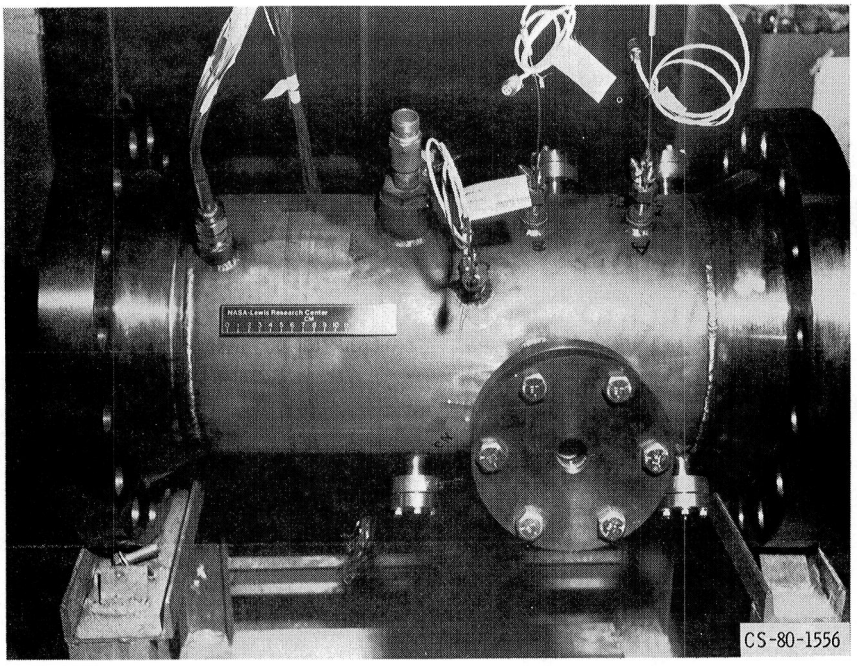

Figure 3. - Combustor housing/heat flux transducer installation.

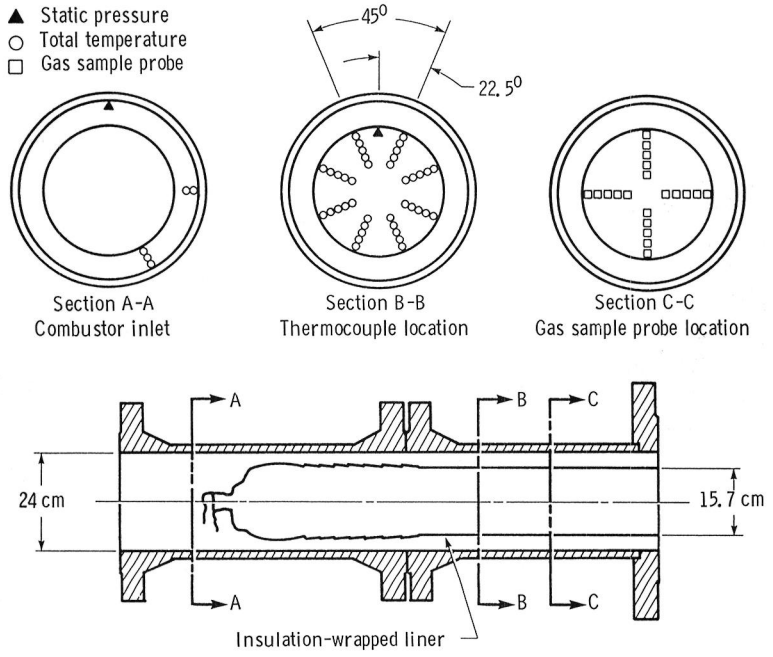

Figure 4. - Combustor assembly and instrumentation sections.

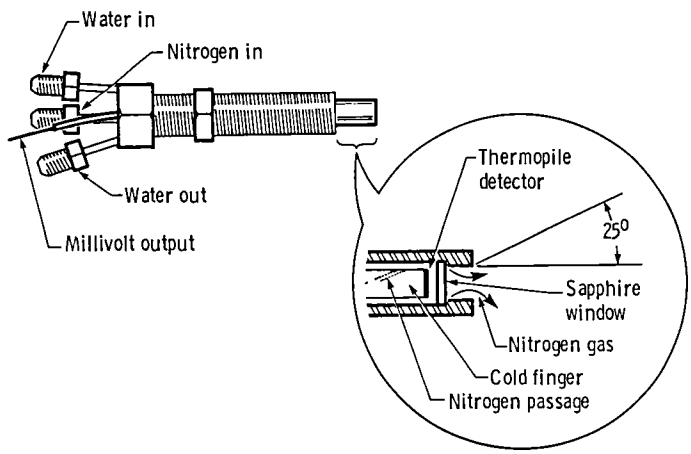

Figure 5. - Hot wall radiometer.

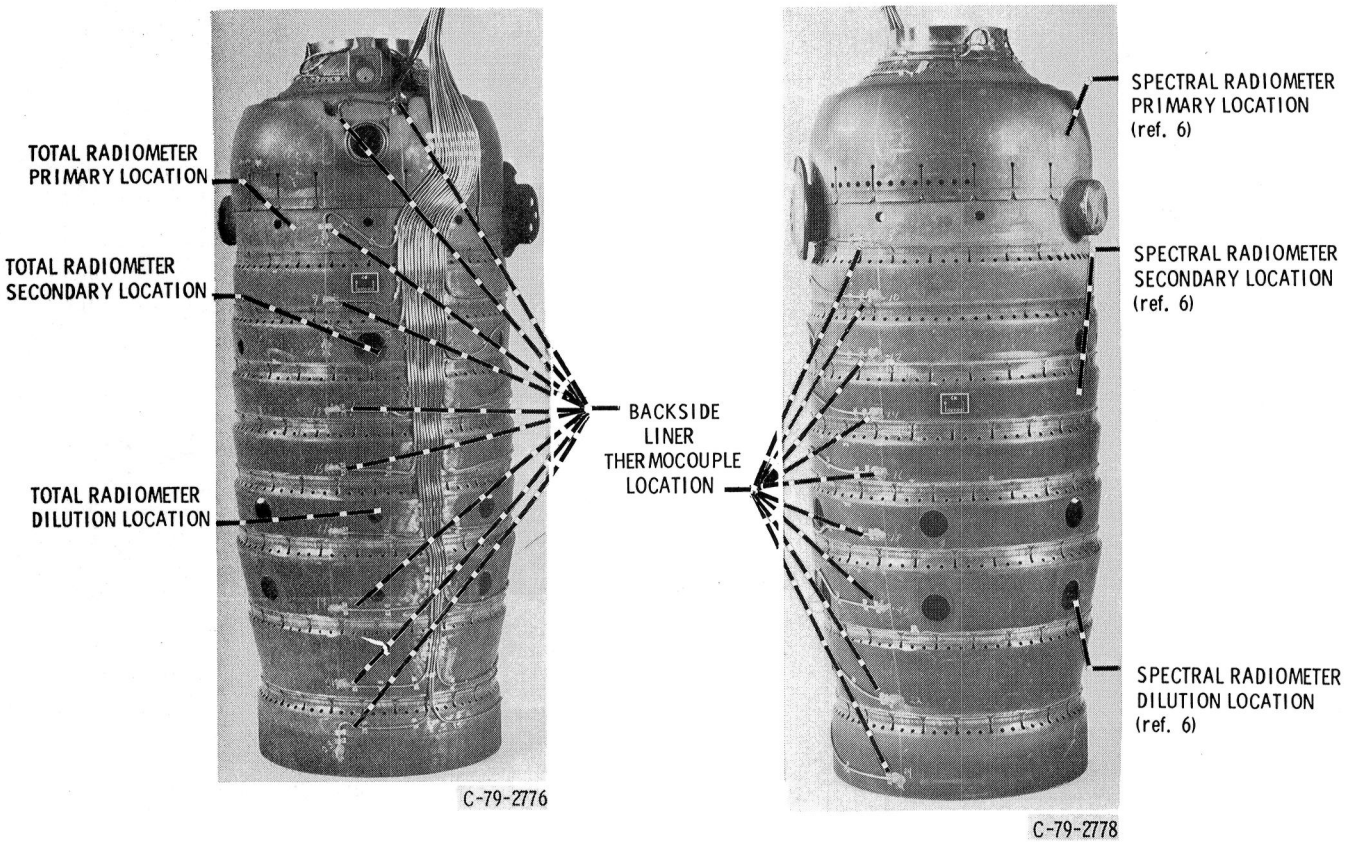

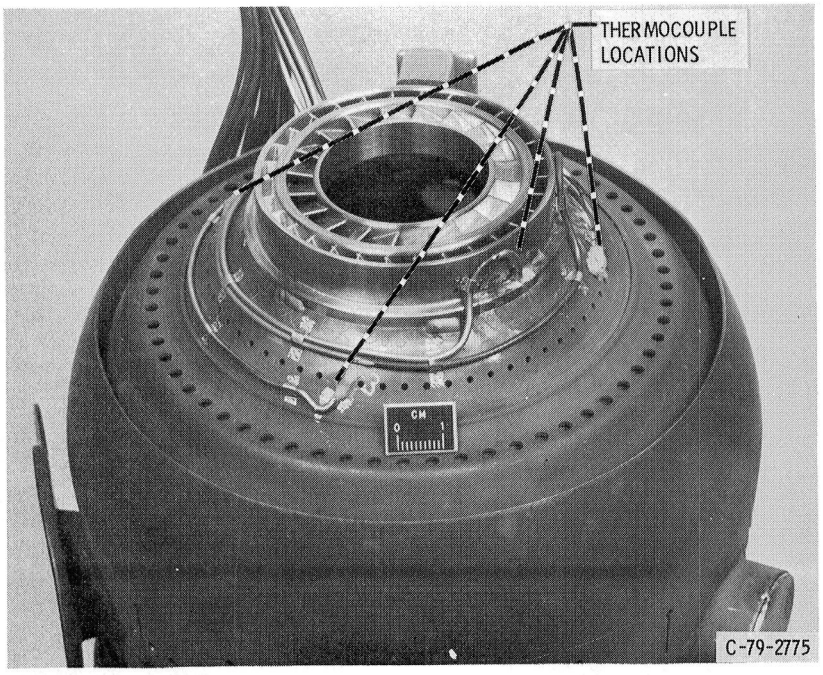

Figure 6. - Backside thermocouple & radiometer locations.

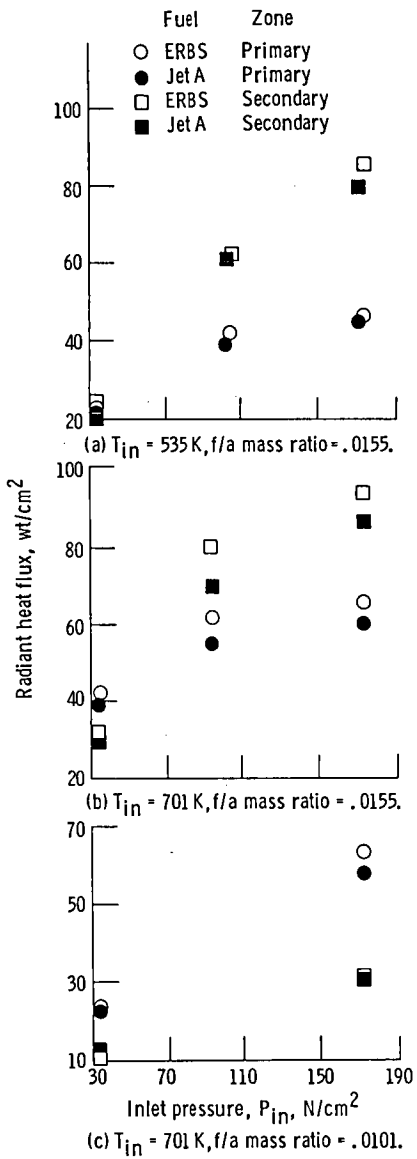

Figure 7. - Pressure effects on radiant heat flux.

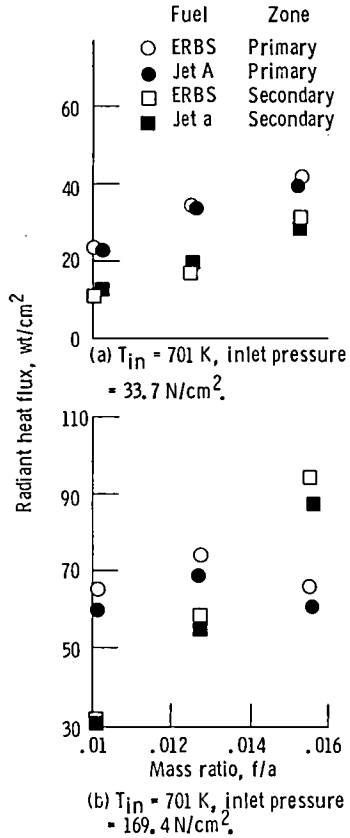

Figure 8. - Fuel/air mass ratio effects on radiant heat flux.

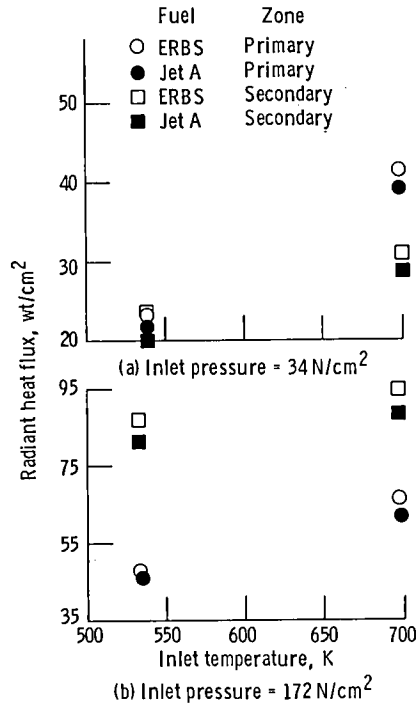

Figure 9. - Effect of inlet air temperature on radiant heat flux at a f/a mass ratio of .0154.

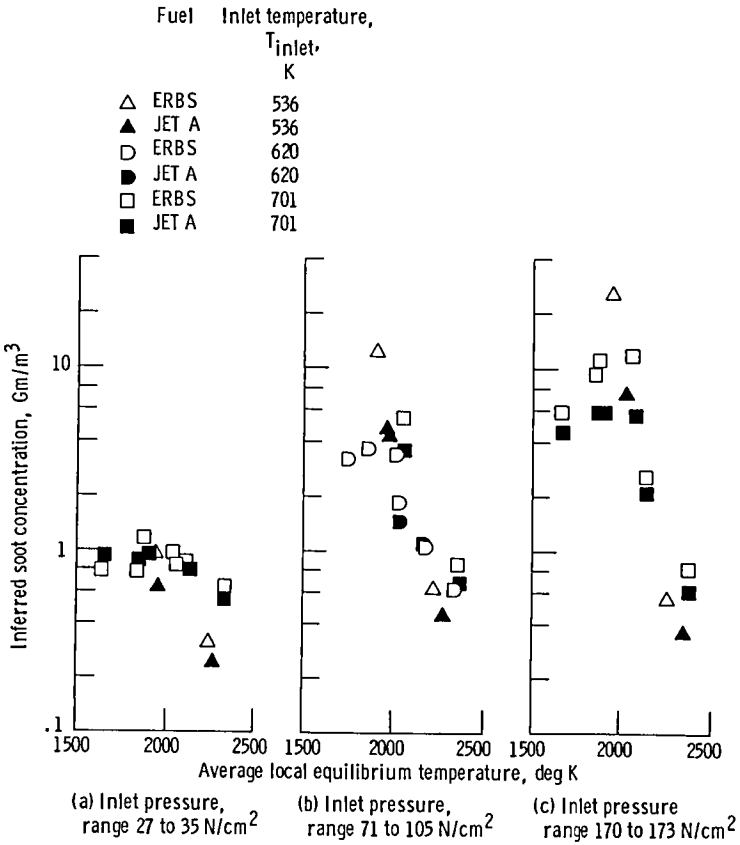

Figure 10 - Behavior of inferred soot concentration with local equilibrium temperature.

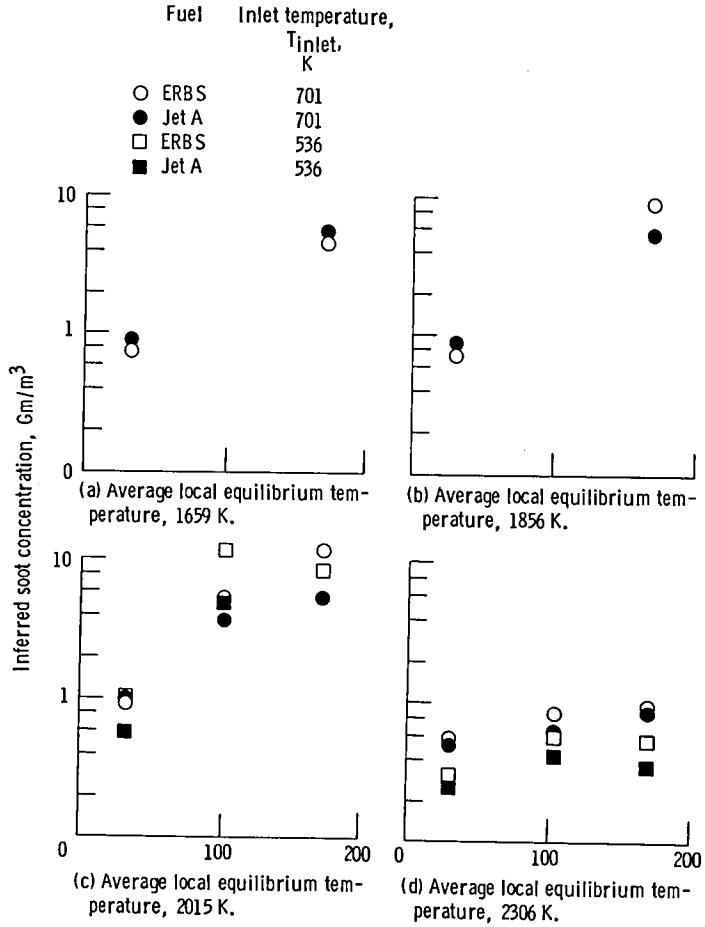

Figure 11. - Behavior of inferred soot concentration with pressure.

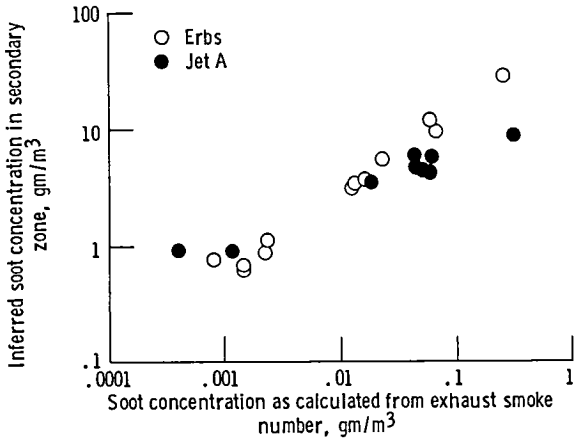

Figure 12. - Correlation of inferred soot concentration with SAE exhaust smoke number.

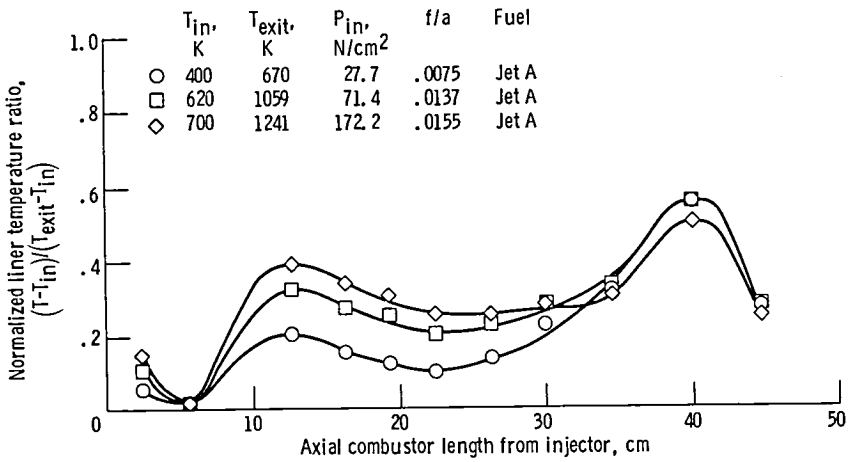

Figure 13. - Typical normalized liner temperature profiles.

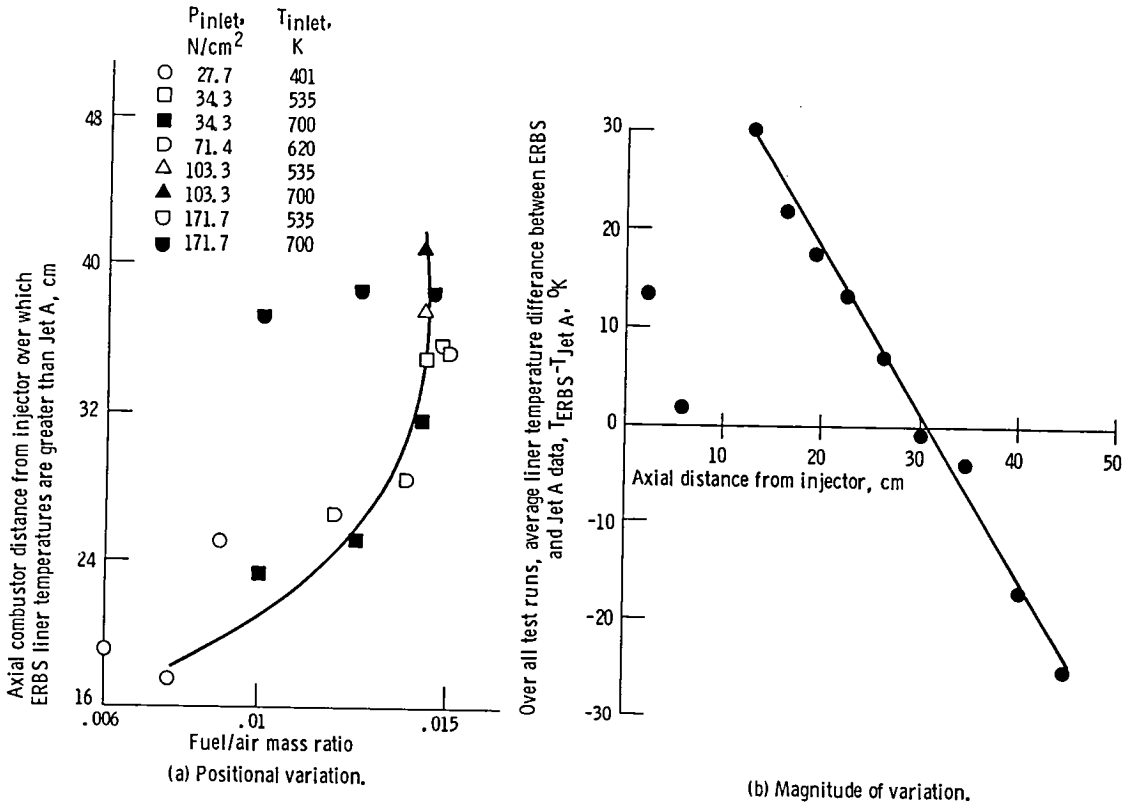

Figure 14. - Comparisons between backside liner temperatures using Jet A and ERBS fuel.

1. Report No.	2. Government Accession No.	3. Recipient's Catalog No.
NASA TM-83537		

4. Title and Subtitle	5. Report Date
Effects of Broadened Property Fuels on Radiant Heat Flux to Gas Turbine Combustor Liners	December 1983
	6. Performing Organization Code: 505-31-42
7. Author(s): John B. Haggard, Jr.	8. Performing Organization Report No.: E-1906
	10. Work Unit No.
9. Performing Organization Name and Address: National Aeronautics and Space Administration, Lewis Research Center, Cleveland, Ohio 44135	11. Contract or Grant No.
	13. Type of Report and Period Covered: Technical Memorandum
12. Sponsoring Agency Name and Address: National Aeronautics and Space Administration, Washington, D.C. 20546	14. Sponsoring Agency Code

15. Supplementary Notes

16. Abstract

The effects of fuel type, inlet air pressure, inlet air temperature, and fuel/air ratio on the combustor radiation were investigated. Combustor liner radiant heat flux measurements were made in the spectral region between .14 and 6.5 microns at three locations in a modified commercial aviation can combustor. Two fuels, Jet A and a heavier distillate research fuel called ERBS were used. The use of ERBS fuel as opposed to Jet A under similar operating conditions resulted in increased radiation to the combustor liner and hence increased backside liner temperature. This increased radiation resulted in liner temperature increases always less than 73°C. The increased radiation is shown by way of calculations to be the result of increased soot concentrations in the combustor. The increased liner temperatures indicated can substantially affect engine maintenance costs by reducing combustor liner life up to 1/3 because of the rapid decay in liner material properties when operated beyond their design conditions.

17. Key Words (Suggested by Author(s))	18. Distribution Statement
Soot formation Gas turbine combustors Flame radiation	Unclassified - unlimited STAR Category 28

19. Security Classif. (of this report)	20. Security Classif. (of this page)	21. No. of pages	22. Price*
Unclassified	Unclassified		

*For sale by the National Technical Information Service, Springfield, Virginia 22161